Theoret. Comput. Sci. 980 (2023) 114247

Contents lists available at ScienceDirect

Theoretical Computer Science

journal homepage: www.elsevier.com/locate/tcs

Feasibility assessments of a dynamical approach to compartmental modelling on graphs: Scaling limits and performance analysis ☆

Ethan Hunter *, Jessica Enright, Alice Miller

School of Computing Science, University of Glasgow, Glasgow, G12 8QQ, Scotland, United Kingdom

ARTICLE INFO

Keywords:
Epidemiology
Graph theory
Dynamical systems
Monte Carlo

ABSTRACT

Sharkey, Kiss and others developed a dynamical approach to modelling epidemic disease on a contact graph by generating systems of first-order ordinary differential equations expressing the model dynamics [1,2], which are solved to yield exact and deterministic modelling results. However, they left algorithmic generation (and solving) of systems and runtime assessment of the approach as an open question. To address this, we give an open source implementation that takes both a compartmental model and a contact graph as input and then generates and solves a system of equations exactly describing the dynamics of the system. Our implementation uses a moment closure result on single-vertex cutsets in the contact graph to reduce the number of equations required. In runtime experiments, we find that the implementation of the dynamical approach is almost always slower than a comparable Monte Carlo simulation in finding the expected state of the modelling system at a specified time. To complement our runtime evaluations, we give results and bounds on the number of equations required to describe a system as a function of the size of the compartmental model and input graph. We show that a natural extension of the moment closure result on single-vertex cutsets to larger cutsets is only possible for restricted projections of the model states on the cutset. We conclude that the dynamical approach is unlikely to be suitable unless exact, deterministic (rather than simulated) results are essential.

1. Introduction

Compartmental models have enjoyed broad popularity in modelling diseases since their introduction [3]. Recent applications have particular relevance to the COVID-19 pandemic, such as the evaluation of models of pandemic evolution [4] and development of vaccination strategies [5]. However, traditional compartmental models implicitly assume homogeneous populations, where results relate to the portions of the population in each model state at given time-steps [6]. To extend compartmental modelling frameworks to heterogeneous contact processes, we can use contact graphs (networks) to represent population structures, e.g. [7–9].

In this paper, we evaluate and improve on a dynamical approach to compartmental models on contact graphs, first presented in [1] and developed in [2,10–13]. This approach uses exact, deterministic systems of equations to describe the dynamics of SIR models on contact graphs.

☆ This article belongs to Section C: Theory of natural computing, Edited by Lila Kari.

* Corresponding author.
E-mail address: e.hunter.2@research.gla.ac.uk (E. Hunter).

https://doi.org/10.1016/j.tcs.2023.114247
Received 15 May 2023; Received in revised form 21 September 2023; Accepted 6 October 2023

Available online 12 October 2023

1.1. Contribution

Our main contributions are as follows. In section 3.1, we obtain an upper bound on the number of equations in a system describing an SIR model on a contact graph showing that such systems scale at most exponentially in the number of vertices in the contact graph. Therefore in general this dynamical approach is unlikely to be practical. However, in section 3.2, expanding on a result on paths using moment closures in [2], we show that for an SIR model on a tree on n vertices, the size of the system scales linearly in n (and is in fact exactly $5n-3$). In section 3.3, we consider a more complex compartmental model than the SIR example on trees to understand how systems scale not only with number of vertices in the contact graph but also with complexity of the compartmental model. In particular, we use the upper bound in section 3.2 to show that system size scales polynomially in the worst case in model complexity. In section 3.4 we generalise an existing exact moment closures result in [2] on single cut-vertices to larger cutsets but show that this only holds under restricted projections of the model states.

The authors of a key improvement of the dynamical approach [2] noted that "generating and implementing the equations needed for an exact description is prone to error and we *highly recommend the development of an algorithmic approach*" (italics our own). We have addressed this in Section 4 by providing an implementation that generates, with or without the moment closure result in Section 2.2.3, and solves these equations (our implementation can be accessed at https://github.com/Ethan-CS/DynamicalGraphModel). We perform runtime measurements using this implementation for models on random graphs with two aims. In section 4.2 we compare the performances of our implementation and a Monte Carlo method on the same parameters, finding that a Monte Carlo simulation almost always finds the expected state of the modelling system at a specified time faster than generating and solving equations. In section 4.3 we find that the use of moment closures expands the range of densities of graph for which the dynamical approach is practical.

2. Background

In this section, we provide an overview of the dynamical approach that we build on in subsequent sections. We define compartmental models and in particular the classical SIR model before explaining how the SIR framework can be used to model disease on contact graphs. We then demonstrate an exact moment closure result from [2] that reduces the size of dynamical systems involved in modelling SIR models on certain graph classes.

2.1. Preliminaries

Due to the interdisciplinary nature of our work, we note some standard graph theory definitions that are used throughout. A *digraph* (or *directed graph*) $G=(V,E)$ is a pair composed of a finite set V called the *vertices* and an irreflexive binary relation on V called an *adjacency relation* represented as a set E of ordered pairs of vertices $\{(v_i,v_j) \mid v_i,v_j \in V\} \subseteq V \times V$ called the *edges*. An *undirected graph* $G=(V,E)$ is a digraph in which the adjacency relation is symmetric i.e., $E=E^{-1}$. Unless otherwise stated, we use undirected graphs and refer to them simply as "graphs." While we define the following notions on graphs, we could analogously define them on digraphs.

A *weighted graph* (G,w) is pair composed of a graph $G=(V,E)$ and a weight function $w : E \to \mathbb{R}$, where $w(e)$ is the *weight* of edge $e \in E$. For a graph $G=(V,E)$, a *subgraph* $H=(V_H,E_H)$, denoted $H \subseteq G$, is a graph on a vertex-set $V_H \subseteq V$ and edge-set $E_H = \{\{v_i,v_j\} \mid v_i,v_j \in V_H\} \subseteq E$. An *induced subgraph* is a graph on a vertex-set $V_H \subseteq V$ and an edge-set consisting of all edges $\{v_i,v_j\} \in E$ for $v_i,v_j \in V_H$. The subgraph of G induced by V_H is denoted $G[V_H]$. A *component* of a graph G is an induced subgraph $G[V_H] \subseteq G$ such that the graphs $G[V_H]$ and $G \setminus G[V_H]$ are *disconnected* i.e., for any vertices v_i and v_j in G and $G[V_H]$ respectively, there is no sequence of pairwise connected vertices $(v_i, v_{i+1}, \ldots, v_j)$. A component $C \subseteq G$ is a maximal connected induced subgraph of G.

2.1.1. Compartmental models

We now define the preliminaries of compartmental models, including transition digraphs and interaction functions which will allow us to define how individuals progress through disease states during the evolution of models.

Definition 2.1 *(Interaction function).* Let X be a set of model states and let A and B be subsets of $X \times X$. An interaction function is a function $\texttt{inter} : A \to B$ such that, for $(a_i,a_j) \in A$ and $(b_k,b_l) \in B$, $\texttt{inter}(a_i,a_j) = (b_k,b_l)$ indicates that interaction between individuals in states a_i and a_j can lead to state transitions $a_i \mapsto b_k$ and $a_j \mapsto b_l$.

For example, in Section 2.2.1 we show the interaction function for the SIR model, which defines a single interaction: a susceptible and an infected individual coming into contact can lead to the susceptible individual becoming infected.

Definition 2.2 *(Transition digraph).* A transition digraph $(T=(X,E),w)$ is a weighted digraph on a set of model states X where the directed edge set E defines how individuals progress through disease states for a particular disease and where the weight function w gives the rates at which these transitions occur.

As an example, Fig. 1 shows the transition digraph for the SIR model, which we define in Section 2.2. Note that we use interaction functions in combination with transition digraphs to define models, meaning that the rate of infection β in Fig. 1 is not fixed.

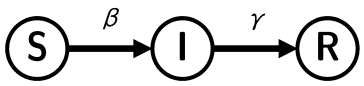

Fig. 1. Transition digraph for the SIR compartmental model, in which individuals are initially susceptible S and move to infected I with rate β before moving to recovered R with rate γ.

Definition 2.3 *(Compartmental model).* A compartmental model $M((T, w), \texttt{inter}, N)$ is a triple composed of a transition digraph T with weight function w, an interaction function `inter` and a population of integer size $N > 0$.

The dynamics of compartmental models are given by a system of differential equations describing the rates at which members of the population transition between the states of the transition digraph.

We now present an important example of a compartmental model and an extension to graph-based population structures.

2.2. The SIR model

The SIR Model is a compartmental model defined on the transition digraph shown in Fig. 1 with population size N. Individuals are divided into three populations as follows:

- *susceptible*: these individuals do not currently have the infection, but could contract it, and are said to be in state S;
- *infected*: these individuals have the disease, are infectious and are said to be in state I; and
- *recovered*: these individuals have recovered from the disease, now have immunity from it and are said to be in state R.

This model is used throughout this paper, so we now define it formally.

2.2.1. The classical model

Let $T = ((X, E), w)$ be the transition digraph with function w depicted in Fig. 1 on states $X = \{S, I, R\}$, let $\texttt{inter} : A \to B$ be an interaction function on $A, B \subseteq X \times X$ that defines a single interaction $(S, I) \mapsto (I, I)$ and let N be a positive integer. Then, an SIR model is the triple $M((T, w), \texttt{inter}, N)$. To write differential equations for the dynamics of M, let $S(t)$, $I(t)$ and $R(t)$ be the numbers of *susceptible*, *infected* and *recovered* individuals respectively at time t. We require that, at any time t, $S(t) + I(t) + R(t) = N$ when vital dynamics (births and deaths) are not considered. Let β be the average number of contacts per person multiplied by the probability of transmission and let γ be the reciprocal of the average length of time that an infected individual remains infected. Then, the dynamics of the model M are given by the following system of first-order ODEs [3]:

$$\frac{dS}{dt} = -\beta \frac{SI}{N} \tag{1}$$

$$\frac{dI}{dt} = \beta \frac{SI}{N} - \gamma I \tag{2}$$

$$\frac{dR}{dt} = \gamma I \tag{3}$$

2.2.2. Graph-based model

Traditional compartmental models such as the SIR model as defined by equations (1)-(3) implicitly assume a well-mixed population i.e., homogeneous mixing of a homogeneous population [6]. This means that traditional models return unrealistic results when the rate at which individuals come into contact with one another varies significantly across the population, which is closer to reality for many modelling use cases. Contact graphs can be informed by techniques and results from Social Network Analysis to provide more realistic representations of populations [14].

Definition 2.4 *(Contact graph).* A contact graph $(G = (V, E), w)$ is a weighted graph in which each vertex $v \in V$ represents an individual member of a population and an edge $\{v_i, v_j\} \in E$ is a 'potentially transmitting contact' through which disease can be transmitted between v_i and v_j, and $w(\{v_i, v_j\})$ gives the probability per timestep of transmission for the edge.

Generally, models of disease using contact graphs obtain modelling results by averaging the results of many stochastic simulations from a single set of initial conditions - this is called a Monte Carlo approach [15]. In contrast, the dynamical approach from [1] yields a system of differential equations, which are exact descriptions of the model dynamics and not specific to any one set of initial conditions. These equations can be solved to understand the time-evolution of subsystem probabilities from particular initial conditions.

We show how the SIR modelling framework can be applied to contact graphs [1]. First, we define notation and terminology for the probability of an event and its time-derivative, beginning with a generalisation of Definition 2.3 to include contact graphs.

Definition 2.5 *(Compartmental model on a contact graph).* A compartmental model M is a triple $((T, w), \texttt{inter}, G)$ composed of a weighted transition digraph (T, w), an interaction function `inter` and a contact graph $G = (V, E)$.

The dynamics of compartmental models on contact graphs can be defined by systems of differential equations where each equation describes the rate of change of the probability of a set of contact graph vertices[1] being in a set of model states, formally referred to as a *moment*.

Definition 2.6 *(Moment).* Let M be a compartmental model with a transition digraph $T = (X, E)$ on a contact graph $G = (V, E)$. Let σ be a sequence

$$\sigma = (\sigma^{i_1})_{j_1}, (\sigma^{i_2})_{j_2}, \dots, (\sigma^{i_r})_{j_r}$$

where, for $1 \leq l \leq r$, $\sigma^{i_l} \in X$ and $j_l \in V$. Then, $\langle\sigma\rangle(t)$ - denoting the probability that for each $1 \leq l \leq r$, each vertex j_l is in the model state σ^{i_l} at time t - is referred to as a moment of order r. The rate of change of $\langle\sigma\rangle(t)$ with respect to t is denoted $\langle\dot{\sigma}\rangle(t)$

For example, consider a model M and a graph G. Let $r = 3$, let i_1, i_2, i_3 be the vertices labelled 1, 2 and 3 and let j_1, j_2 and j_3 be the model states S, I and S. Then, $\langle\sigma\rangle(t)$ represents the probability that at time t, the vertices 1, 2 and 3 are in states S, I and S respectively i.e., $\langle S_1 I_2 S_3\rangle$.

An adjacency matrix A for a contact graph on n vertices is an $[n \times n]$ matrix where A_{ij} is the weight of the edge between v_i and v_j i.e., the probability of infection between vertices v_i and v_j (which is zero if there is no edge between v_i and v_j). We are rarely interested in self-infection so usually set A_{ii} to be zero for all vertices v_i.

Returning to a SIR model example, for a fixed rate of recovery for all vertices γ, we can write the expressions for the time derivatives of the probabilities of each vertex v_i being in each state S, I and R respectively as moments of order one as follows:

$$\langle \dot{S}_i \rangle = -\sum_{j=1}^{N} A_{ij} \langle S_i I_j \rangle$$

$$\langle \dot{I}_i \rangle = \sum_{j=1}^{N} A_{ij} \langle S_i I_j \rangle - \gamma_i \langle I \rangle$$

$$\langle \dot{R}_i \rangle = \gamma_i \langle I \rangle,$$

as given in [1]. These equations constitute the 'singles-based model,' which is an approximate representation of the system dynamics. An exact representation of the model dynamics requires equations for moments of order up to the number of vertices in the contact graph [1], as follows. Begin with equations for moments of order one and proceed recursively: derive an equation for the time derivative of each moment appearing in the equations previously derived until moments of order equal to the size of the contact graph are reached.

Each of these equations for particular subsystem states are derived from the master (Kolmogorov) equation from [1], for which we use the following shorthand notation for subsystem states on several vertices.

Notation 2.1 *(Shorthand for subsystem states).* From Definition 2.6, let $\mathcal{Z} = \sigma_{i_1}, \sigma_{i_2}, \dots, \sigma_{i_r}$ and $W = j_1, j_2, \dots, j_r$. Then, we write the sequence σ in Definition 2.6 as $W^{\mathcal{Z}}$ and moment $\langle\sigma\rangle(t)$ as $\langle W^{\mathcal{Z}}\rangle(t)$.

For example, in an SIR model on a contact graph with at least three vertices, if $W = (v_1, v_2, v_3)$ and $\mathcal{Z} = (S, I, S)$, then $W^{\mathcal{Z}}$ is the subsystem projection in which vertex v_1 is in state S, vertex v_2 is in state I and v_3 is in state S. The probability of this subsystem projection is denoted $\langle W^{\mathcal{Z}}\rangle = \langle S_1 I_2 S_3\rangle$.

Let M be a compartmental graph model with transition digraph $T = (X, E)$ on a contact graph $G = (V, E)$, and $\mathcal{A}, \mathcal{Z}$ be sequences of length $|V|$ comprised of states in X. Let $\varsigma^{\mathcal{Z}\mathcal{A}}$ be the probability per timestep of transition from $V^{\mathcal{A}}$ to $V^{\mathcal{Z}}$ and similarly let $\varsigma^{\mathcal{A}\mathcal{Z}}$ be the probability per timestep of transition from $V^{\mathcal{Z}}$ to $V^{\mathcal{A}}$. Then, the master equation (giving the rate of transition to the system state projection $V^{\mathcal{Z}}$) for the dynamical system describing the model M is

$$\langle \dot{V^{\mathcal{Z}}} \rangle = \sum_{\mathcal{A}} \varsigma^{\mathcal{Z}\mathcal{A}} \langle V^{\mathcal{A}} \rangle - \sum_{\mathcal{A}} \varsigma^{\mathcal{A}\mathcal{Z}} \langle V^{\mathcal{Z}} \rangle. \tag{4}$$

An analogous equation can be derived for subsystem states [1].

For example, consider an SIR model (as previously defined) on the lollipop graph $L = (V, E)$ shown in Fig. 2. For a full description of this model, by following the procedure outlined in [1] and using equation (4), we require 35 equations [2] for the following moments (the full equations have been provided in Appendix A.1):

Order 1: $\langle S_1\rangle, \langle I_1\rangle, \langle S_2\rangle, \langle I_2\rangle, \langle S_3\rangle, \langle I_3\rangle, \langle S_4\rangle, \langle I_4\rangle$

Order 2: $\langle S_1 I_2\rangle, \langle S_1 I_3\rangle, \langle S_1 I_4\rangle, \langle I_1 S_2\rangle, \langle I_1 S_3\rangle, \langle S_3 I_4\rangle, \langle I_3 S_4\rangle, \langle I_1 S_4\rangle$

Order 3: $\langle S_1 S_3 I_4\rangle, \langle S_1 I_2 I_3\rangle, \langle S_1 I_3 I_4\rangle, \langle S_1 I_2 I_4\rangle, \langle S_1 I_3 S_4\rangle, \langle S_1 S_2 I_3\rangle,$

[1] We refer to contact graph vertices and individuals interchangeably.

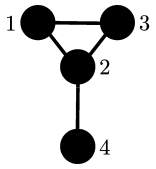

Fig. 2. The lollipop graph.

$$\langle S_1S_2I_4\rangle, \langle I_1S_3I_4\rangle, \langle S_1I_2S_3\rangle, \langle I_1S_3S_4\rangle, \langle I_1I_3S_4\rangle, \langle S_1I_2S_4\rangle$$

Order 4: $\langle S_1I_2S_3I_4\rangle, \langle S_1I_2I_3I_4\rangle, \langle S_1I_2I_3S_4\rangle, \langle S_1S_2I_3I_4\rangle,$

$$\langle S_1S_2S_3I_4\rangle, \langle S_1S_2I_3S_4\rangle, \langle S_1I_2S_3S_4\rangle$$

We refer to this method of equation generation as a bottom-up approach. We could instead write down equations for all possible terms in a top-down fashion, which would lead a lot more equations.

Having shown how the equations in a dynamical system describing an SIR model on a contact graph are generated, we now introduce a result that can reduce the size of this system.

2.2.3. Exact moment closures

In a dynamical system, equations for higher-order moments contain terms for (and thus depend upon) lower-order moments; introducing *moment closures* allows us to select a moment for which all higher-order moments are no longer in the system. This may be because higher-order terms are ignored, leading to an approximate system, or because they are written in terms of existing, lower-order terms, which may preserve the exact system dynamics. A system of equations without moment closures is referred to as a *full* system; a system in which moment closures are used is referred to as a *closed* system. Note that closures in our context are exact for graphs containing cycles only if cycles in the graph are preserved under closures [2] - we ensure this is the case by first identifying cut vertices in graphs, then introducing closures for terms referencing these vertices case-by-case, meaning cycle structures are not broken.

As we show in Section 3.2, the size of the system of equations scales at worst exponentially in the size of the contact graph. To reduce this scaling in systems describing SIR models on graphs of certain classes, we can use the main result from [2]. This result exploits cut vertices to reduce the number of equations required to describe a compartmental model on a graph. The main idea is to write higher-order moments in the full system that reference cut-vertices as products of other, lower-order moments.

Theorem 2.1. *[2] Let $G = (V, E)$ be a graph. Consider a connected subset of vertices $F \subseteq V$ and assume that F contains a cut-vertex v_{i*} such that $F \setminus \{v_{i*}\}$ can be separated into two non-empty vertex sets F_1 and F_2, where the subgraphs induced by F_1 and F_2 are each composed of at least one distinct component and there are no edges from F_1 to F_2. Then, for any sets of states $\mathcal{X}$ and $\mathcal{Y}$ of lengths $|F_1|$ and $|F_2|$ respectively, the following holds:*

$$\langle F_1^{\mathcal{X}} S_{v_{i*}} F_2^{\mathcal{Y}}\rangle(t) = \frac{\langle F_1^{\mathcal{X}} S_{v_{i*}}\rangle\langle S_{v_{i*}} F_2^{\mathcal{Y}}\rangle(t)}{\langle S_{v_{i*}}\rangle(t)}.$$

Moment closures can be approximations for the full system dynamics if we are simply discarding moments over a given order [16]. However, it is shown in [2] that Theorem 2.1 defines *exact* moment closures.

Returning to the lollipop graph example in Fig. 2, observe that vertex 2 is a cut-vertex. The closure result from Theorem 2.1 allows us to close moments that reference this cut-vertex. For example, the moment $\langle S_1S_2I_3\rangle$ can be closed:

$$\langle S_1S_2I_3\rangle = \frac{\langle S_1S_2\rangle\langle S_2I_3\rangle}{\langle S_2\rangle}.$$

This moment contains a term that we did not require in the system before closures - $\langle S_1S_2\rangle$. In the SIR model, all-susceptible terms are not dynamically relevant as they do not lead to a change of state. However, as this term appears in a term that arises by application of the expression in 2.1, an exact description of the system dynamics therefore requires an equation for this term. For the SIR model on a contact graph $G = (V, E)$, such terms are only those in all-susceptible subsystem state projections, which lead to an increase of at most $|E|$ equations in the system [2].

By applying moment closures, the closed - but still full and exact - system of equations required to describe an SIR model on the lollipop graph is given by the following moments (and equations given in Appendix A.2):

$$\langle S_1\rangle, \langle I_1\rangle, \langle S_2\rangle, \langle I_2\rangle, \langle S_3\rangle, \langle I_3\rangle, \langle S_4\rangle, \langle I_4\rangle$$

$$\langle S_1I_2\rangle, \langle S_1I_3\rangle, \langle S_1I_4\rangle, \langle I_1S_2\rangle, \langle I_1S_3\rangle, \langle S_3I_4\rangle, \langle I_3S_4\rangle, \langle I_1S_4\rangle, \langle S_1S_2\rangle, \langle S_1S_3\rangle, \langle S_1S_4\rangle$$

$$\langle S_1S_3I_4\rangle, \langle S_1I_3I_4\rangle, \langle S_1I_3S_4\rangle, \langle S_1I_3I_4\rangle, \langle I_1S_3S_4\rangle, \langle I_1I_3S_4\rangle, \langle S_1S_3S_4\rangle$$

The numbers of equations required to describe an SIR model with and without closures on the lollipop graph and some other common small graphs (including the bowtie and bowtie-with-bridge graphs - see Fig. 3) are given in Table 1, to illustrate the

Table 1
Numbers of equations required for full descriptions of an SIR model on different graphs with and without exact moment closures on single cut-vertices.

Graph	Full	Closed	Reduction
Path on 3 vertices	13	12	7.7%
Path on 30 vertices	1336	685	48.7%
Lollipop	35	26	25.0%
Bowtie	89	40	55.0%
Bowtie with Bridge	119	73	38.7%

(a) The Bowtie Graph (b) The Bowtie-with-Bridge Graph

Fig. 3. The Bowtie and Bowtie-with-Bridge Graphs.

extent to which closures can reduce the numbers of equations. These values have been obtained using our dynamical approach implementation.

3. Bounds and results on system sizes

We investigate the theoretical advantages offered by moment closures by first deriving an upper bound on system size for an SIR model on a general graph. We then derive results for system sizes with and without moment closures for three specific graph classes and give a result for a more complex compartmental model on a tree. We provide runtime experiment results to demonstrate the practical impact of the theoretical results regarding moment closures obtained.

3.1. Upper bound on system size

Notation 3.1. Let M be a compartmental model. We denote by $N_{eq}(M,G)$ the size of the full system of equations describing the dynamics of M on a contact graph G. Similarly, we denote by $N'_{eq}(M,G)$ the size of the closed system.

Let $M((T,w),\texttt{inter},G)$ be a compartmental graph model on a set of model states X and a vertex set V. We derive an initial upper bound on $N_{eq}(M,G)$ by observing that the number of equations for moments of order i is bounded above by $\binom{|V|}{i}|X|^i$, since there are $|X|^i$ ways to arrange $|X|$ states on i vertices and $\binom{|V|}{i}$ ways to combine i vertices. Hence, as $\sum_{i=0}^{|V|}\binom{|V|}{i}a^{|V|-i}b^i=(a+b)^{|V|}$,

$$N_{eq}(M,G)\leq\sum_{i=1}^{|V|}\binom{|V|}{i}|X|^i=(|X|+1)^{|V|}-1 \tag{5}$$

Therefore, in the worst case $N_{eq}(M,G)$ scales *exponentially* in $|V|$. Therefore, in general the dynamical modelling approach is tractable only for graphs on small numbers of vertices. To address this, we discuss results for system sizes on restricted graph classes, with special attention paid to graphs to which we can apply moment closures on cut vertices.

3.2. System sizes for specific graph classes

We note the following encouraging bound for the size of systems describing SIR models on tree-like graphs.

Result 3.1. *[2] Let G be a graph on n vertices and e edges with t cycles on three vertices and no cycles on more than three vertices and let $M((T,w),\texttt{inter},G)$ be an SIR model. Then,*

$$N'_{eq}(M,G)\leq 2n+3e+7t\leq 10n$$

Hence, the size of closed systems for SIR models on this restricted graph class scales *linearly* with the number of graph vertices. For a contact graph $G=(V,E)$, we can use a depth-first search to identify cut-vertices in $O(|V|+|E|)$ time [17], thus, the entire procedure to generate a closed system of equations on such tree-like graphs will take time that is linear in the number of vertices and edges in the contact graph. This only relates to generation of equations - we later discuss the complexity of solving these equations, for which a standard numerical method takes $O(n^3)$ time to solve n equations.

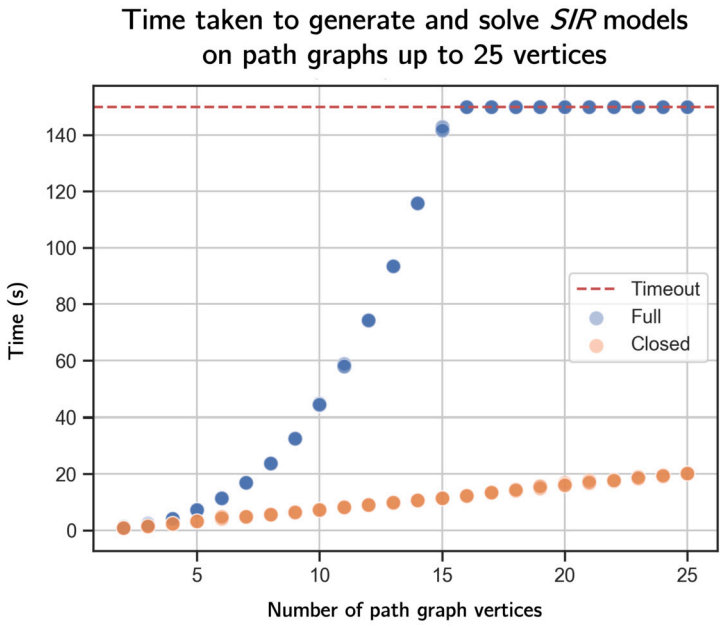

Fig. 4. Comparison of time taken to generate and solve full and closed systems for SIR models on path graphs up to 25 vertices, where five models were solved for each length of path. The timeout of 150 seconds is indicated by a dashed red line. (For interpretation of the colours in the figure(s), the reader is referred to the web version of this article.)

3.2.1. SIR model on trees

We first consider the subclass of graphs considered in Result 3.1 in which $t = 0$ i.e., trees. Note that the results in this section are specific to the restricted graph class of trees precisely because the structure of trees allows us to exploit as far as possible closures on cut-vertices, since every vertex of degree greater than one in a tree is a cut-vertex. In better-connected graphs than trees, using closures on cut-vertices becomes decreasingly fruitful - we illustrate this with the example of cycle graphs, which contains no cut-vertices although each vertex is of low degree (two).

Definition 3.1 *(Tree).* A tree is an undirected, connected graph with no cycles.

The first class of tree we consider is the path graph.

Definition 3.2 *(Path Graph).* A path graph $P_n = (V, E)$ is a graph on a vertex set $V = v_1, v_2, \ldots, v_n$ and edge set $E = \{\{v_i, v_{i+1}\} \mid i = 1, 2, \ldots, n-1\}$.

In [2], the following result for path graphs is presented without proof.

Result 3.2. *[2] For an SIR model M on a path graph P_n,*

$$N_{eq}(M, P_n) = (3n^2 - n + 2)/2, \text{ and}$$

$$N'_{eq}(M, P_n) = 5n - 3.$$

When generating a closed system of equations, the implementation identifies cut-vertices in the contact graph and for any moment of order three or more in which a cut-vertex appears, the code instead adds the relevant product of lower-order moments by application of the expression in Theorem 2.1. Fig. 4 shows a comparison of runtimes for our implementation of the dynamical approach to obtain results for full and closed systems defining the dynamics of an SIR model on path graphs with up to 25 vertices.

Existing algorithms for numerically solving dynamical systems run in time that is at worst cubic in system size [18], so reducing the input size for the solver using moment closures significantly decreases the time taken to solve these systems. For reference, using our implementation the average time taken to generate and solve the system of equations for an SIR model on P_{50} without closures (3,726 equations) was 4.58 seconds and with closures (247 equations) was 0.67 seconds, a runtime decrease of 85.4%.

In Appendix C, for completeness we prove the expression from Result 3.2 for the size of the full system. Rather than prove the result for the closed system size, we instead prove a generalisation to trees. For this, we use a corollary of Theorem 2.1.

Result 3.3. *[2] For an SIR model on a tree T_n with $n \geq 3$ vertices, the following moment closures hold for all vertices v_i, v_j and v_k inducing in T_n a connected subgraph in which v_j is a cut-vertex:*

$$\langle S_i S_j I_k \rangle = \frac{\langle S_i S_j \rangle \langle S_j I_k \rangle}{\langle S_j \rangle} \quad \text{and} \quad \langle I_i S_j I_k \rangle = \frac{\langle I_i S_j \rangle \langle S_j I_k \rangle}{\langle S_j \rangle}.$$

This follows from the observation that all vertices in a tree with degree greater than 1 are cut-vertices. From Result 3.1, since for a tree $t = 0$ and the number of edges (e) is $(n-1)$, the number of equations in the reduced system is at most $5n-3$. In Theorem 3.1, we strengthen this result to equality:

Theorem 3.1. *Let M be an SIR model. Then, for a tree T_n on n vertices,*

$$N'_{eq}(M, T_n) = 5n - 3.$$

Proof. We require $2n$ moments of order one: for each $v_i \in V$, they are equations for $\langle \dot{S}_i \rangle$ and $\langle \dot{I}_i \rangle$. Since the number of edges in T_n is $n-1$, we require $3(n-1)$ moments of order two, which from Result 3.3 are the equations for $\langle \dot{S_i} I_j \rangle$, $\langle I_i \dot{S_j} \rangle$ and $\langle \dot{S_i} \dot{S_j} \rangle$. Using Result 3.3, the reduced system contains moments of order at most two. Therefore, the number of equations in the reduced system describing an SIR model on T_n is $2n + 3(n-1) = 5n - 3$. ■

3.2.2. SIR model on cycle graphs

Inspired by Theorem 3.1, we derive an expression for the number of equations required to describe an SIR model on a *cycle graph* on n vertices defined as follows:

Definition 3.3 *(Cycle Graph).* A cycle graph $C_n = (V, E)$ is a graph with vertex set $V = v_1, v_2, \ldots, v_n$ and edge set $E = \{\{v_{i \bmod n}, v_{(i+1) \bmod n}\} \mid i = 1, 2, \ldots, n\}$.

To prove a result on the number of equations in an SIR system on a cycle on n vertices, we require the following lemma.

Lemma 3.2. *There are n paths of length $0 < l < n$ in a cycle graph C_n.*

Proof. The proof of this result is obvious: consider each path of length l with lowest-indexed vertex v_i for $1 \leq i < n$. ■

In Theorem 3.3, we consider the number of equations required to describe the dynamics of an SIR model on a cycle graph. Note that cycle graphs do not contain any single cut-vertices, so system size cannot be reduced using single cut-vertex moment closures.

Theorem 3.3. *Let M be an SIR model. For a cycle graph C_n with $n \geq 3$,*

$$N_{eq}(M, C_n) = N'_{eq}(M, C_n) = 3n^2 - 3n.$$

Proof. First, consider the number of equations for moments of order one. For an SIR model, for each vertex v_i we require one equation for the susceptible case $\langle S_i \rangle$ and one for the infected case $\langle I_i \rangle$, so there are $2n$ equations for single vertex states in total, two for each of the n vertices.

For moments of order two, there are n pairs of adjacent vertices $\{v_i, v_j\}$ in a cycle and two dynamically interesting states, $\langle S_i I_j \rangle$ and $\langle I_i S_j \rangle$ as these are the only two state combinations for a connected pair of vertices that could lead to a change of state, so we require $2n$ equations for moments of order two.

Consider terms of length $3 \leq l < n$. The sequences of vertices in moments of order l are precisely the paths of length l in the cycle because we only require equations for moments on vertices constituting connected subgraphs in the contact graph. This is because moments on more than one induced subgraph would be equivalent to the product of the moments on each of the subgraphs, as these events are independent. By similar reasoning, it is shown in [2] that moments including two adjacent infected vertices do not occur in the system of equations as no further pairwise transmission can occur through the edge. Hence, up to indexing there are precisely three dynamically relevant subsystem states for a set of vertices inducing a path of length $3 \leq l < n$:

$$\langle S_{i \bmod n} S_{(i+1) \bmod n} \cdots S_{(i+l-2) \bmod n} I_{(i+l-1) \bmod n} \rangle, \tag{6}$$

$$\langle I_{i \bmod n} S_{(i+1) \bmod n} \cdots S_{(i+l-2) \bmod n} S_{(i+l-1) \bmod n} \rangle, \tag{7}$$

$$\langle I_{i \bmod n} S_{(i+1) \bmod n} \cdots S_{(i+l-2) \bmod n} I_{(i+l-1) \bmod n} \rangle. \tag{8}$$

By Lemma 3.2, there are n paths of each length $3 \leq l < n$ on a cycle. Hence, there are a total of $n(n-3)$ paths of lengths $3 \leq l < n$ in a cycle. Given also that there are 3 moments of orders $3 \leq l < n$ as in equations (6)-(8), there are $3n(n-3)$ moments on $3 \leq l < n$ vertices in the system of equations describing an SIR model on a cycle.

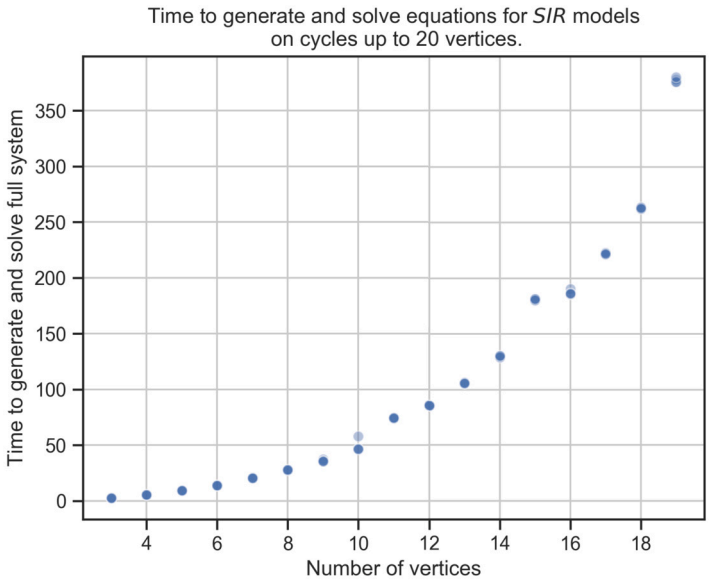

Fig. 5. Time taken to generate and solve systems of equations for SIR models on cycle graph up to 20 vertices. Five models were solved for each cycle.

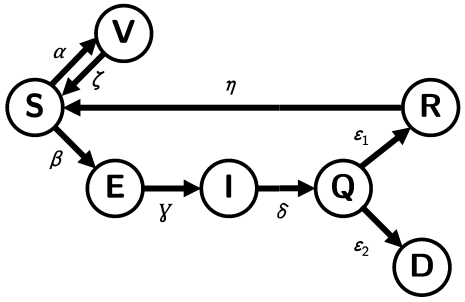

Fig. 6. Transition digraph of the $SEIQRDV$ compartmental model [19].

Finally, we consider terms on n vertices. Notice that the subsystem of states shown in equations (6) and (7) on all n vertices of the cycle overlap, so we need only consider one of these cases. Therefore, since there are n paths on n vertices in the cycle $(v_{i \bmod (n)}, v_{(i+1) \bmod (n)}, \dots, v_{(i+n) \bmod (n)})$, there are $2n$ equations for terms describing subsystem states of length n. Hence, in total we have $2n + 2n + 3n(n-3) + 2n = 3n^2 - 3n$ equations in the system describing the dynamics of an SIR model on a cycle graph, as required. ■

Fig. 5 shows runtime results for our dynamical modelling implementation on cycles up to 20 vertices.

3.3. $SEIQRDV$ model on trees

While equation (5) implies that system sizes scale exponentially in the contact graph size in the worst case, it also implies that systems scale polynomially in the number of model states (even in the worst case). Hence, the dynamical approach may be useful when studying more complex compartmental models, although we are aware that in most cases the contact graph will be far larger than the model. We discuss the example of an $SEIQRDV$ model, used to model the impact of social distancing and vaccination measures on the spread of COVID-19 [19]. In the $SEIQRDV$ model, individuals can be in the following states:

- susceptible (S): these individuals can contract the infection;
- exposed (E): these individuals have been in contact with either an exposed or infected person and are not displaying clinical symptoms but can infect others;
- infected (I): these individuals have the infection, are displaying symptoms and are infectious;
- quarantined (Q): these individuals have the infection but cannot infect;
- recovered (R): these individuals have had the infection and are no longer infectious - they have decaying immunity and return to the susceptible state when this is zero;
- deceased (D): these individuals have contracted the infection and died as a result; and

- vaccinated (V): these individuals have obtained a vaccine and are have decaying immunity, returning to susceptible when this is zero.

The transition digraph of this model is given in Fig. 6. We show in Theorem 3.4 that system size scales linearly in contact graph vertices for an $SEIQRDV$ model on a tree.

Theorem 3.4. *Let M be an $SEIQRDV$ model in which the susceptible state is not re-entered (i.e., no immunity decay). For a tree T_n on $n > 3$ vertices,*

$$N'_{eq}(M, T_n) = 19n - 13.$$

Proof. The system of equations describing an $SEIQRDV$ model M on a tree $T_n = (V, E)$ contains terms for each vertex $v_i \in V$ being in state other than deceased (as moments for individual vertices in this state can be found through complements) of the transition digraph of the model, as in Fig. 6. These moments are $\langle S_i\rangle, \langle E_i\rangle, \langle I_i\rangle, \langle Q_i\rangle, \langle R_i\rangle$ and $\langle V_i\rangle$. Hence, $6n$ equations for the derivatives of moments of order one are required.

The only state that is left through interaction with a neighbouring contact graph vertex in the model is S (through interaction with states E and I). Thus, higher-order moments are introduced to the system by appending to a lower-order moment an S term or another term that can enter S and a term that can induce a change of state for a neighbour in S - other transitions do not lead to moments of increasing order. Since the contact graph is a tree, the system has no moments of order 3 or higher by analogous arguments to those of Result 3.1, so we need only consider moments of order up to 2. Hence, for each edge in the tree we require moments for the incident vertices being in states: SE and ES, SI and IS, VE and EV, VI and IV, RE and ER, RI and IR and finally SS. Thus, the system contains a total of $13|E| = 13(n-1)$ moments of order two, as T_n has $(n-1)$. Hence,

$$N'_{eq}(M, T_n) = 6n + 13(n-1) = 19n - 13. \quad \blacksquare$$

3.4. Closures on larger cutsets

We considered a generalisation of Theorem 2.1 for cutsets larger than one vertex.

Definition 3.4 *(Cutset).* Let $G = (V, E)$ be a connected graph. A cutset of G is a vertex-set $C \subset V$ such that the graph $G[V \setminus C]$ is disconnected.

For an SIR model in which the susceptible state cannot be re-entered, when sets of vertices are susceptible, no transmission has occurred through these vertices. In particular, if the vertices of a cutset are all susceptible, the states of the subgraphs that are disconnected by removal of the cutset remain independent. Where at least one cutset vertex is in a state other than susceptible, the probabilities of the components disconnected by cutset removal are dependent, which explains why the above proposition does not hold. We can expand this notion using the following definition.

Definition 3.5 *(Outlet state).* For a compartmental model M on a set of states X, a state $x \in X$ is called an outlet state if individuals in the model can only exit this state, not enter it from another state during the evolution of the model.

For the SIR models considered in this paper, the susceptible state cannot be entered from any other state, making susceptible an outlet state.

The following generalisation to Theorem 2.1 is generalised not only to cutsets of more than one vertex but also to any static compartmental model, provided there exists at least one outlet state in the model. In an SIR model, it is shown in [2] that cut-vertices only ever appear in moments in the susceptible state, so Theorem 2.1 is a corollary of the following theorem when the size of the cutset is one.

Theorem 3.5. *Let $M((T, w), \texttt{inter}, G = (V, E))$ be a compartmental model. Consider a connected subset of vertices $F = \{v_1, v_2, \dots, v_k\} \subseteq V$ and assume that F contains a cutset $C = \{v_l, v_{l+1}, \dots, v_{l+m}\} \subset F$ such that $F \setminus C$ is partitioned into at least two disjoint components $F_1 = \{v_1, v_2, \dots, v_{l-1}\}$ and $F_2 = \{v_{l+m+1}, v_{l+m+2}, \dots, v_k\}$. Let $\mathcal{O}$ be a sequence of outlet model states and $\mathcal{X}_1, \mathcal{X}_2$ be sequences of model states. Then, the following is an exact moment closure result:*

$$\langle F_1^{\mathcal{X}_1} C^{\mathcal{O}} F_2^{\mathcal{X}_2}\rangle(t) = \frac{\langle F_1^{\mathcal{X}_1} C^{\mathcal{O}}\rangle\langle C^{\mathcal{O}} F_2^{\mathcal{X}_2}\rangle(t)}{\langle C^{\mathcal{O}}\rangle(t)}.$$

Proof. Note the subgraphs spanned by F_1 and F_2 are disjoint with no other links except via the cutset C. As the vertices of C are all in all-outlet states, transmission through the cutset has not occurred and the projections of the system state on F_1 and F_2 represent independent events. By the Kolmogorov definition of conditional probabilities [20],

$$\langle F_1^{\mathcal{X}_1} C^{\mathcal{O}} F_2^{\mathcal{X}_2}\rangle = \langle F_1^{\mathcal{X}_1} C^{\mathcal{O}} F_2^{\mathcal{X}_2} | C^{\mathcal{O}}\rangle\langle C^{\mathcal{O}}\rangle,$$

which, using the independence of F_1 and F_2, can be written as

$$\langle F_1^{\mathcal{X}_1} C^{\mathcal{O}} F_2^{\mathcal{X}_2} | C^{\mathcal{O}} \rangle = \langle F_1^{\mathcal{X}_1} C^{\mathcal{O}} | C^{\mathcal{O}} \rangle \langle C^{\mathcal{O}} F_2^{\mathcal{X}_2} | C^{\mathcal{O}} \rangle$$

Again, using the definition of conditional probabilities we have

$$\frac{\langle F_1^{\mathcal{X}_1} C^{\mathcal{O}} F_2^{\mathcal{X}_2} \rangle}{\langle C^{\mathcal{O}} \rangle} = \frac{\langle F_1^{\mathcal{X}_1} C^{\mathcal{O}} \rangle \langle C^{\mathcal{O}} F_2^{\mathcal{X}_2} \rangle}{\langle C^{\mathcal{O}} \rangle^2}$$

i.e.,

$$\langle F_1^{\mathcal{X}_1} C^{\mathcal{O}} F_2^{\mathcal{X}_2} \rangle = \frac{\langle F_1^{\mathcal{X}_1} C^{\mathcal{O}} \rangle \langle C^{\mathcal{O}} F_2^{\mathcal{X}_2} \rangle}{\langle C^{\mathcal{O}} \rangle}$$

as required. ■

When generating equations, cutsets of size two or more in terms are not guaranteed to be in outlet states, unlike single vertex cutsets (cut-vertices) which only appear in outlet states [2]. We prove the following proposition to show that terms referencing the cutset in states other than outlet states cannot be exactly closed. This means the reduction in system size for this moment closure result is in general less than that of Theorem 2.1.

Proposition 3.1. *Let $G = (V, E)$ be a graph and consider a connected subset of vertices $F \subseteq V$. Assume that F contains a cutset C on $l < k$ vertices such that the graph $G[F \setminus C]$ is partitioned into at least two non-empty vertex sets F_1 and F_2, where the graphs $G[F_1]$ and $G[F_2]$ are each composed of at least one distinct component and there are no edges between them. Then, for sequences of model states $\mathcal{X}_1, \mathcal{X}_2$ and $\mathcal{X}_3$, the following is not necessarily an exact moment closure:*

$$\langle F_1^{\mathcal{X}_1} C^{\mathcal{X}_2} F_2^{\mathcal{X}_3} \rangle(t) = \frac{\langle F_1^{\mathcal{X}_1} C^{\mathcal{X}_2} \rangle \langle C^{\mathcal{X}_2} F_2^{\mathcal{X}_3} \rangle(t)}{\langle C^{\mathcal{X}_2} \rangle(t)}. \tag{9}$$

Proof. For a contradiction, let M be a discrete-time SIR model on a graph G with a vertex set $\{v_1, v_2, v_3, v_4\}$ and edge set $\{\{v_1, v_2\}, \{v_1, v_3\}, \{v_2, v_3\}, \{v_2, v_4\}, \{v_3, v_4\}\}$. Let the probabilities of infection and recovery be uniformly given by $1/2$. Let M have initial conditions as follows: at time $t = 0$,

$$\langle S_1 \rangle = 1 \tag{10}$$

$$\langle S_2 \rangle = 1 \tag{11}$$

$$\langle S_3 \rangle = 1 \tag{12}$$

$$\langle S_4 \rangle = 0. \tag{13}$$

i.e., vertex 4 is infected and the other vertices are susceptible. Then, by $t = 1$ vertices 3 is infected with probability $1/2$ and similarly for vertex 4. Assume that by time $t = 3$,

$$\langle S_1 S_2 I_3 I_4 \rangle = \frac{\langle S_1 S_2 I_3 \rangle \langle S_2 I_3 I_4 \rangle}{\langle S_2 I_3 \rangle}. \tag{14}$$

Given the initial conditions in equations (10)-(13), it is a simple task to find the following probabilities at time $t = 3$:

$$\langle S_1 S_2 I_3 I_4 \rangle = 7/128$$

$$\langle S_1 S_2 I_3 \rangle = 1/8$$

$$\langle S_2 I_3 I_4 \rangle = 5/64$$

$$\langle S_2 I_3 \rangle = 9/16$$

and thus, again at time $t = 3$,

$$\langle S_1 S_2 I_3 I_4 \rangle \neq \frac{\langle S_1 S_2 I_3 \rangle \langle S_2 I_3 I_4 \rangle}{\langle S_2 I_3 \rangle},$$

since $7/128 \neq (1/8 \times 5/64)/(9/16) = 5/288$. ■

The closure expression in Theorem 3.5 is derived directly from the Kolmogorov definition of conditional probabilities, so the result holds because the states of the cutset and subgraphs are independent. When this is not true, for example in an SIR model in which individuals can return to the susceptible state or in the case of Proposition 3.1, no closure result - even on single-vertex cutsets - would be possible as no outlet state exists.

4. Empirical results

To understand the dynamical approach empirically, we conduct experiments on Erdős-Rényi random graphs. After expaining the algorithmic procedure used to generate and solve equations, we use our implementation to comparing runtimes when generating and solving full and closed systems to understand the practical impact of moment closures. We then present runtime comparisons of the dynamical approach and a Monte Carlo implementation. We find that solving the full system is practically infeasible for all but very sparse graphs, where we expect only a handful of edges, as models on graphs generated with edge probability $p > 0.1$ all timed out at 60 seconds. We show that the closed system can be solved for slightly more highly connected graphs but often times out (at 60 seconds) for graphs with average degree 4 or more - a significant improvement on the full system, but difficult to justify in most practical settings as 25 vertices is a very small graph. We now show how this dynamical approach with moment closures compares in runtime to an analogous Monte Carlo approach, which supports this conclusion.

4.1. Implementation

The first equations generated are those for single-vertex terms: a complete representation of the system dynamics includes equations for each vertex in each non-terminal model state. The equations for each term are determined using the master equation - this involves considering model projections that could lead into and out of the model projection represented by each term. Then, we recursively add to the system equations for moments of terms that have been added in previous equations (for example, if an equation for $\langle S_1 \rangle$ includes the term $\langle S_1 I_2 \rangle$, we now need to add an equation for the latter) until we have written an equation for each term in the right hand side of any other equations. Pseudocode for this implementation is provided in Algorithm 1.

The implementation is written in Python and publicly available here: https://github.com/Ethan-CS/DynamicalGraphModel. We use the LSODA solver from ODEPACK, a suite of solvers written in FORTRAN [21]. This is able to quickly detect and switch between nonstiff and stiff methods for solving systems of differential equations using a method outlined in [22]. A dynamical system problem is stiff if the solution being sought varies slowly but has close solutions that vary very quickly, meaning a numerical solver needs to take small steps to obtain correct results, and nonstiff otherwise.

Example 4.1. Consider inputting into Algorithm 1 an SIR model on a path on three vertices, with vertices labelled 1, 2 and 3 and edges $\{1,2\}$ and $\{2,3\}$. At line 2, we assign to the variable `non_terminal_states` the list $[S, I]$. At lines 4-6, the set `rhs_terms` is assigned the value

$$\{[(S,1)],[(S,2)],[(S,3)],[(I,1)],[(I,2)],[(I,3)]\}.$$

Taking the first (and only) pair of the first term gives $(\sigma, v) \leftarrow (S,1)$. At line 12 the variable `interact_states` for state S is assigned the value $\{I\}$ and on line 13 we assign $\rho \leftarrow I$, its only value for this term. This is an out-neighbour of S in the transition digraph of the SIR model we consider, so we go to line 18. In lines 19 and 20, we assign $\tau \leftarrow I$ and $r \leftarrow \beta_v$, the rate of infection for v (potentially time-dependent, depending on model definition). The only neighbour of vertex 1 in the path on 3 vertices is the vertex 2, so in line 21 we assign $w \leftarrow 2$ and this is not already in `term`. Then, in line 23 `new_term` is assigned to the value $[(S,1),(I,2)]$. We cannot close this term (while 2 is a cut-vertex, it does not contain 3 or more state-vertex pairs) so we go to line 34, where `eq_terms` (the equation for the term $[(S,1)]$) is updated with the term $-\beta_v * [(S,1),(I,2)]$. We add this equation to the dictionary `system` in line 38, with the key being $[(S,1)]$ and the value `eq_terms`. We remove $[(S,1)]$ from `rhs_terms` in line 39 now it has an equation in `system` and add $[(S,1),(I,2)]$ to `rhs_terms` in lines 40-42. The variable `rhs_terms` now has the value

$$\{[(S,2)],[(S,3)],[(I,1)],[(I,2)],[(I,3)],[(S,1),(I,2)]\}$$

so we return to line 10, repeating the procedure until this list is empty.

Further in the process, we reach line 25 having assigned to `new_term` the value $[(S,1),(S,2),(I,3)]$ - this contains a cut-vertex (vertex 2) and is of length 3, so the closure result in Theorem 2.1 can be applied. In line 26, $V \leftarrow [1,2,3]$ and in line 27 (ς, c) is $(S,2)$. We assign $F_1 \leftarrow [1]$ and $F_2 \leftarrow [2]$ in line 28 so lines 29-31 yield the assignment

$$\texttt{new\_term} \leftarrow [(S,1),(S,2)] * [(S,2),(I,3)]/[(S,2)].$$

This is multiplied by the relevant rate of transition and added to the relevant equation in line 37.

The resulting system of 12 equations outputted by this procedure for an SIR model on a path on three vertices, which corresponds to the system of equations in Appendix B, is:

$$\begin{aligned}
\frac{d}{dt}[(S,0)] &= -\beta_{1,0} * [(S,0),(I,1)] \\
\frac{d}{dt}[(S,1)] &= -\beta_{0,1} * [(I,0),(S,1)] - \beta_{2,1} * [(S,1),(I,2)] \\
\frac{d}{dt}[(S,2)] &= -\beta_{1,2} * [(I,1),(S,2)] \\
\frac{d}{dt}[(I,0)] &= \beta_{1,0} * [(S,0),(I,1)] - \gamma_0 * [(I,0)]
\end{aligned}$$

Algorithm 1 Generate equations for a model M on a graph G where $M = [((T, w), \mathcal{I}, G = (V, E)]$ comprises: a weighted transition digraph (T, w); an interaction function describing interaction between states $\mathcal{I}$, and a contact graph G.

procedure GENERATEEQUATIONS(model $M[((T, w), \mathcal{I}, G = (V, E)])$ ▷ as in Definition 2.5
  non_terminal_states ← $[\sigma \in T \mid \texttt{out\_degree}(\sigma) > 0]$
  rhs_terms ← { }
  for each vertex v in G **do**
    for each state σ in non_terminal_states **do**
      append $[(\sigma, v)]$ to rhs_terms ▷ corresponds to $\langle \sigma_v \rangle$
    end for
  end for
  system ← [ ]
  while rhs_terms not empty **do**
    for each term in rhs_terms **do**
      eq_terms ← [ ]
      for each (σ, v) in term **do**
        interact_states ← $\{\rho \mid \{\rho, \sigma\} \in$ domain of $\mathcal{I}\} \cup \{n \mid n$ a neighbour of σ in $T\}$
        for each ρ in interact_states ∩ non_terminal_states **do**
          if ρ is an in-neighbour of σ **then** ▷ i.e. there is an edge from ρ to σ in E
            $r \leftarrow$ transition rate of $(\sigma, v) \mapsto (\rho, v)$ calculated from M
            new_term ← term with (σ, v) replaced by (ρ, v)
            add $r *$ new_term to eq_terms
          else if $\{\rho, \sigma\}$ in domain of $\mathcal{I}$ **then**
            $\tau \leftarrow$ resulting state for σ interacting with ρ
            $r \leftarrow$ transition rate of $(\sigma, v) \mapsto (\tau, v)$ calculated from M
            for each neighbour w of v **do**
              if w is not in term **then** ▷ introduce closure terms - see Theorem 2.1
                new_term ← term ∪ (ρ, w)
                if $\exists \in$ new_term such that x is a cut-vertex in G **and** length new_term ≥ 3 **then**
                  $V \leftarrow [v \mid (\epsilon, v) \in$ term$]$
                  $(\varsigma, c) \leftarrow$ state-vertex pair of cut-vertex c in term
                  lists $F_1, F_2 \leftarrow$ vertices of components of $G[V \setminus \{c\}]$
                  new_term_1 ← vertices of F_1 and c in original states from term
                  new_term_2 ← vertices of F_2 and c in original states from term
                  new_term ← new_term_1 $*$ new_term_2$/(\varsigma, c)$
                end if
              else
                new_term ← term with state of w replaced by ρ
              end if
              add $-r *$ new_term to eq_terms
            end for
          else
            $r \leftarrow$ transition rate of $(\sigma, v) \mapsto (\rho, v)$ calculated from M
            add $-r *$ term to eq_terms
          end if
        end for
      end for
      update system with d/dt(term) = eq_terms
      remove term from rhs_terms
      for new_term in eq_terms **do**
        if no equation for new_term in system **then**
          add new_term to rhs_terms
        end if
      end for
    end for
  end while
  return system
end procedure

$$\frac{d}{dt}[(I,1)] = \beta_{0,1} * [(I,0),(S,1)] + \beta_{2,1} * [(S,1),(I,2)] - \gamma_1 * [(I,1)]$$

$$\frac{d}{dt}[(I,2)] = \beta_{1,2} * [(I,1),(S,2)] - \gamma_2 * [(I,2)]$$

$$\frac{d}{dt}[(S,0),(I,1)] = -\beta_{1,0} * [(S,0),(I,1)] + \beta_{2,1} * [(S,0),(S,1)] * [(S,1),(I,2)]/[(S,1)] - \gamma_1 * [(S,0),(I,1)]$$

$$\frac{d}{dt}[(I,1),(S,2)] = \beta_{0,1} * [(I,0),(S,1)] * [(S,1),(S,2)]/[(S,1)] - \beta_{1,2} * [(I,1),(S,2)] - \gamma_1 * [(I,1),(S,2)]$$

$$\frac{d}{dt}[(I,0),(S,1)] = -\beta_{2,1} * [(I,0),(S,1)] * [(S,1),(I,2)]/[(S,1)] - \beta_{0,1} * [(I,0),(S,1)] - \gamma_0 * [(I,0),(S,1)]$$

$$\frac{d}{dt}[(S,1),(I,2)] = -\beta_{0,1} * [(I,0),(S,1)] * [(S,1),(I,2)]/[(S,1)] - \beta_{2,1} * [(S,1),(I,2)] - \gamma_2 * [(S,1),(I,2)]$$

$$\frac{d}{dt}[(S,0),(S,1)] = -\beta_{2,1} * [(S,0),(S,1)] * [(S,1),(I,2)]/[(S,1)]$$

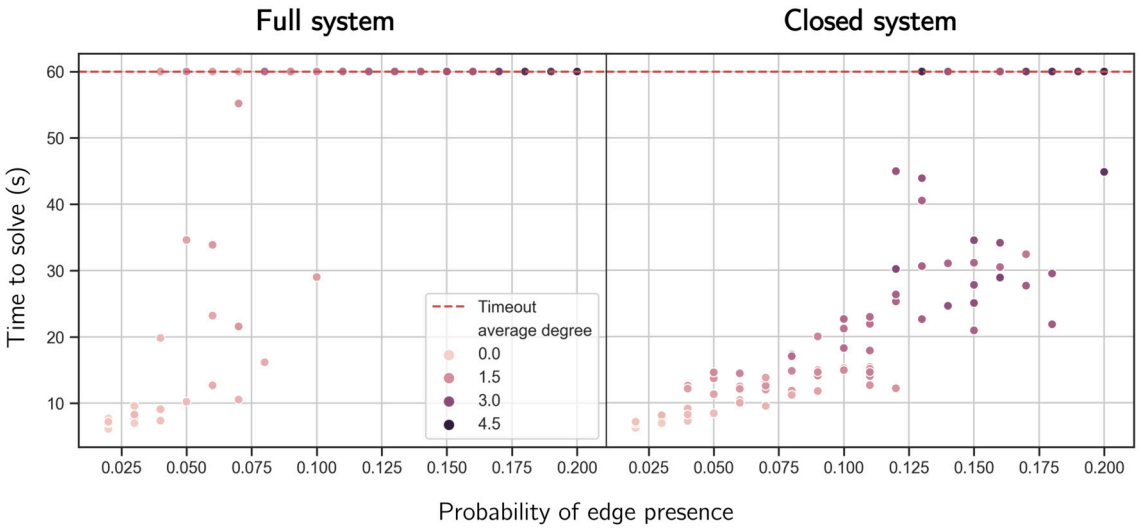

Fig. 7. Time taken to generate and solve full and closed systems of equations for random Erdős-Rényi graphs on 25 vertices and probabilities in the range $0.02 \leq p \leq 0.2$. Point hue indicates mean vertex degree and the timeout of 60 seconds is indicated by a red line.

$$\frac{d}{dt}[(S,1),(S,2)] = -\beta_{0,1} * [(I,0),(S,1)] * [(S,1),(S,2)]/[(S,1)]$$

4.2. Comparison to Monte Carlo simulation

An Erdős-Rényi graph is defined as follows:

Definition 4.1 *(Erdős-Rényi random graph).* [23] An Erdős-Rényi graph $G(n,p)$ is a graph generated on n vertices such that each edge $(v_i, v_j) \in V \times V$ exists with probability p.

Using this graph class allows us to test our approach on graphs of varying density by varying p. An important property of Erdős-Rényi random graphs is the following probability threshold for connectivity:

Result 4.1. *[23] For an Erdős-Rényi graph $G(n,p)$, the value $\ln(n)/n$ is a sharp threshold for the connectivity of G. That is, for any constant $\epsilon > 0$, if $p < \frac{(1-\epsilon)\ln(n)}{n}$, then G is disconnected with high probability and if $p > \frac{(1+\epsilon)\ln(n)}{n}$, the graph is connected with high probability.*

4.3. Moment closures on Erdős-Rényi graphs

Fig. 7 shows plots of runtime measurements for generating and solving full and closed systems of equations on Erdős-Rényi graphs on 25 vertices for edge probabilities between 0.02 and 0.2. Using Result 4.1, we expect Erdős-Rényi graphs on 25 vertices to be disconnected with high probability when $0 \leq p < 0.129$ and connected with high probability when $0.129 < p \leq 1$.

We compare the runtime performance of our implementation of the dynamical approach to a more commonly used alternative, Monte Carlo simulation, which is used to simulate an SIR model for random Erdős-Rényi graphs on 20 vertices for a range of probabilities using repeated random sampling.

For these experiments, we defined the SIR model with all per-link infection rates set as $\beta = 0.7$ and individual recovery rates set as $\gamma = 0.3$. We then generated initial conditions by randomly selecting a vertex to be initially infected, while all other vertices remain susceptible. We used these conditions to solve the model with two different approaches. First, we ran Monte Carlo simulations to time $t = 5$ until the mean results, the set of probabilities with which each graph vertex is infected at time $t = 5$, converged to an average within a tolerance of 1×10^{-3}. We then generated systems of equations with moment closures and solved to the same time-step $t = 5$ for the same initial conditions. The solver was used with a time-step of 0.5, a relative tolerance of 1×10^{-3} and an absolute tolerance of 1×10^{-4}.

Fig. 8 shows that the dynamical approach is always slower than the Monte Carlo approach. While the time taken to solve the dynamical system appears to increase exponentially as the probability used to generate the contact graphs increases, the time taken for the Monte Carlo simulations to produce results seems to increase only slightly as the probability used to generate contact graphs increases. Although many of the graphs generated up to $p = 0.14$ are almost certainly disconnected or tree-like, where the number of equations is polynomial in the number of vertices using moment closures, the Monte Carlo approach is still significantly faster because of the cubic complexity of the numerical solver [18]. In Table 2, we show how much faster the Monte Carlo simulation approach produced results than solving systems of equations on average for each probability in the range - the dynamical approach was never faster.

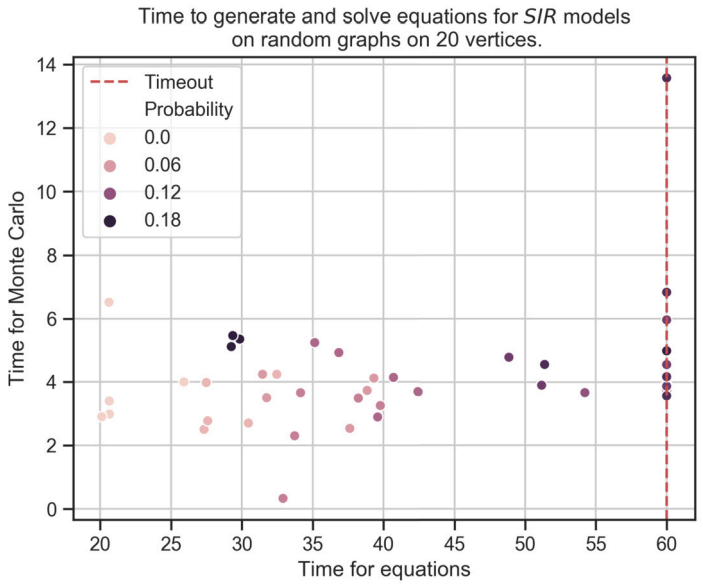

Fig. 8. Comparison of runtime measurements of two approaches to solving an SIR model on Erdős-Rényi graphs on 25 vertices generated on probabilities $0.02, 0.04, \ldots, 0.2)$ for two methods, generating and solving a system of ODEs describing model dynamics and averaging results of Monte Carlo simulations until convergence to within a given tolerance of a self-consistent average. The timeout threshold is indicated, although the Monte Carlo simulation did not reach the threshold. Note that the difference in axes scales is considerable and simulation was always faster than generating and solving equations.

Table 2
Average runtimes, in seconds, for dynamical and simulation approaches to producing results for an SIR model on Erdős-Rényi graphs generated on 20 vertices and probabilities between 0.02 and 0.2 and the difference between these runtimes, where TO indicates all trials on this number of vertices resulted in a timeout.

Generation Probability	Dynamical Runtime (s)	Monte Carlo Runtime (s)	Runtime difference (s)
0.02	21.58	3.96	17.62
0.04	29.07	3.24	25.82
0.06	35.80	3.62	32.18
0.08	35.75	2.61	33.15
0.1	38.94	4.18	34.77
0.12	59.18	3.83	55.35
0.14	56.25	4.61	51.64
0.16	58.72	6.54	52.18
0.18	TO	5.27	-
0.20	TO	5.9	-

5. Discussion and conclusion

We have presented several bounds and expressions as well as empirical results to understand the feasibility of an existing dynamical approach to describing compartmental models on contact graphs which has so far lacked such feasibility analysis. For the use-case of modelling the spread of disease across a graph, we recommend this approach only where one of the following apply: (1) an exact solution to a system is essential, (2) the contact graph is small and tree-like, (3) a Monte Carlo simulation would take equal or greater time to develop than the time taken for existing code to generate and solve the equations for the required system, or (4) numerical integrators improve significantly in efficiency.

We have shown that Monte Carlo simulation can be used in far less time than generating and solving equations to provide the same result as the equation solution. This, we saw, is the case for even very sparse random graphs and even with moment closures. However, we can conceive of some scenarios in which an exact (rather than stochastic) solution is essential, for example in machine learning and artificial intelligence, where the quality, accuracy and reliability of training data has a direct impact on the model. Further, Monte Carlo simulations can be time-consuming to develop, meaning the total time for a stochastic modelling result for some users may be longer, given the dynamical systems can be generated and solved by an existing implementation. This code is publicly available and is capable of generating and solving systems of equations for static compartmental models on general contact graphs. While we did show several promising results on the sizes of systems for particular graph classes, in practice experiments showed that this did not translate to runtimes close to those of Monte Carlo simulation - as we discussed, this is because numerical integrators run in time cubic in the size of the input, so even if the input is small the runtime for solving these equations to some initial conditions can be large. If there is a drastic change in approach for solving systems of equations, including developing a much

more efficient implementation of a numerical method whose complexity is an improvement on cubic in the size of the input, the dynamical approach would benefit greatly and perhaps prove of some further practical usefulness.

There are other methods of estimating epidemic size, for example [24] discusses a method that uses a mean-field approximation based on the degree distribution of a contact graph. While this method does not give probability of infection for any particular vertex in the contact graph where only an approximate overall epidemic size is needed, it would be appropriate to consider this (or other percolation-related approaches e.g. as in [25]). We have not compared the computational efficiency of such methods here, but suggest a comparison to Monte Carlo methods as future work. We would expect that this sort of method would, like the Monte Carlo approach, typically be much faster than the equations-based approach we have considered.

Declaration of competing interest

The authors declare that they have no known competing financial interests or personal relationships that could have appeared to influence the work reported in this paper.

Appendix A. Lollipop example systems

Consider an SIR model on the Lollipop graph of Fig. 2, where each vertex $1, 2, 3, 4$ can be in one of three states S, I, R at a given time t with (for simplicity) uniform rates of infection and recovery β and γ respectively.

A.1. Full system

The full system of equations describing this model is as follows:

$$
\begin{aligned}
\langle \dot{S_1} \rangle(t) &= -\beta\langle S_1 I_2\rangle(t) - \beta\langle S_1 I_3\rangle(t)\\
\langle \dot{S_2} \rangle(t) &= -\beta\langle I_1 S_2\rangle(t) - \beta\langle S_2 I_3\rangle(t) - \beta\langle S_2 I_4\rangle(t)\\
\langle \dot{S_3} \rangle(t) &= -\beta\langle I_1 S_3\rangle(t) - \beta\langle I_2 S_3\rangle(t)\\
\langle \dot{S_4} \rangle(t) &= -\beta\langle I_2 S_4\rangle(t)\\
\langle \dot{I_1} \rangle(t) &= \beta\langle S_1 I_2\rangle(t) + \beta\langle S_1 I_3\rangle(t) - \gamma\langle I_1\rangle(t)\\
\langle \dot{I_2} \rangle(t) &= \beta\langle I_1 S_2\rangle(t) + \beta\langle S_2 I_3\rangle(t) + \beta\langle S_2 I_4\rangle(t) - \gamma\langle I_2\rangle(t)\\
\langle \dot{I_3} \rangle(t) &= \beta\langle I_1 S_3\rangle(t) + \beta\langle I_2 S_3\rangle(t) - \gamma\langle I_3\rangle(t)\\
\langle \dot{I_4} \rangle(t) &= \beta\langle I_2 S_4\rangle(t) - \gamma\langle I_4\rangle(t)\\
\langle I_2 \dot{S_3} \rangle(t) &= -\beta\langle I_1 I_2 S_3\rangle(t) + \beta\langle I_1 S_2 S_3\rangle(t) - \beta\langle I_2 S_3\rangle(t) + \beta\langle S_2 S_3 I_4\rangle(t) - \gamma\langle I_2 S_3\rangle(t)\\
\langle I_1 \dot{S_2} \rangle(t) &= -\beta\langle I_1 S_2 I_3\rangle(t) - \beta\langle I_1 S_2 I_4\rangle(t) - \beta\langle I_1 S_2\rangle(t) + \beta\langle S_1 S_2 I_3\rangle(t) - \gamma\langle I_1 S_2\rangle(t)\\
\langle I_2 \dot{S_4} \rangle(t) &= \beta\langle I_1 S_2 S_4\rangle(t) - \beta\langle I_2 S_4\rangle(t) + \beta\langle S_2 I_3 S_4\rangle(t) - \gamma\langle I_2 S_4\rangle(t)\\
\langle S_2 \dot{I_3} \rangle(t) &= -\beta\langle I_1 S_2 I_3\rangle(t) + \beta\langle I_1 S_2 S_3\rangle(t) - \beta\langle S_2 I_3 I_4\rangle(t) - \beta\langle S_2 I_3\rangle(t) - \gamma\langle S_2 I_3\rangle(t)\\
\langle S_1 \dot{I_3} \rangle(t) &= -\beta\langle S_1 I_2 I_3\rangle(t) + \beta\langle S_1 I_2 S_3\rangle(t) - \beta\langle S_1 I_3\rangle(t) - \gamma\langle S_1 I_3\rangle(t)\\
\langle S_1 \dot{I_2} \rangle(t) &= -\beta\langle S_1 I_2 I_3\rangle(t) - \beta\langle S_1 I_2\rangle(t) + \beta\langle S_1 S_2 I_3\rangle(t) + \beta\langle S_1 S_2 I_4\rangle(t) - \gamma\langle S_1 I_2\rangle(t)\\
\langle S_2 \dot{I_4} \rangle(t) &= -\beta\langle I_1 S_2 I_4\rangle(t) - \beta\langle S_2 I_3 I_4\rangle(t) - \beta\langle S_2 I_4\rangle(t) - \gamma\langle S_2 I_4\rangle(t)\\
\langle I_1 \dot{S_3} \rangle(t) &= -\beta\langle I_1 I_2 S_3\rangle(t) - \beta\langle I_1 S_3\rangle(t) + \beta\langle S_1 I_2 S_3\rangle(t) - \gamma\langle I_1 S_3\rangle(t)\\
\langle S_1 I_2 \dot{I_3} \rangle(t) &= -4\beta\langle S_1 I_2 I_3\rangle(t) + \beta\langle S_1 S_2 I_3 I_4\rangle(t) - 2\gamma\langle S_1 I_2 I_3\rangle(t)\\
\langle I_1 I_2 \dot{S_3} \rangle(t) &= -4\beta\langle I_1 I_2 S_3\rangle(t) + \beta\langle I_1 S_2 S_3 I_4\rangle(t) - 2\gamma\langle I_1 I_2 S_3\rangle(t)\\
\langle S_1 S_2 \dot{I_4} \rangle(t) &= -2\beta\langle S_1 S_2 I_3 I_4\rangle(t) - 2\beta\langle S_1 S_2 I_4\rangle(t) - \gamma\langle S_1 S_2 I_4\rangle(t)\\
\langle I_1 S_2 \dot{I_3} \rangle(t) &= -\beta\langle I_1 S_2 I_3 I_4\rangle(t) - 4\beta\langle I_1 S_2 I_3\rangle(t) - 2\gamma\langle I_1 S_2 I_3\rangle(t)\\
\langle S_2 I_3 \dot{I_4} \rangle(t) &= -\beta\langle I_1 S_2 I_3 I_4\rangle(t) + \beta\langle I_1 S_2 S_3 I_4\rangle(t) - 4\beta\langle S_2 I_3 I_4\rangle(t) - 2\gamma\langle S_2 I_3 I_4\rangle(t)\\
\langle I_1 S_2 \dot{S_4} \rangle(t) &= -\beta\langle I_1 S_2 I_3 S_4\rangle(t) - 2\beta\langle I_1 S_2 S_4\rangle(t) + \beta\langle S_1 S_2 I_3 S_4\rangle(t) - \gamma\langle I_1 S_2 S_4\rangle(t)\\
\langle S_2 S_3 \dot{I_4} \rangle(t) &= -2\beta\langle I_1 S_2 S_3 I_4\rangle(t) - 2\beta\langle S_2 S_3 I_4\rangle(t) - \gamma\langle S_2 S_3 I_4\rangle(t)\\
\langle S_1 I_2 \dot{S_3} \rangle(t) &= -2\beta\langle S_1 I_2 S_3\rangle(t) + \beta\langle S_1 S_2 S_3 I_4\rangle(t) - \gamma\langle S_1 I_2 S_3\rangle(t)\\
\langle S_1 S_2 \dot{I_3} \rangle(t) &= -\beta\langle S_1 S_2 I_3 I_4\rangle(t) - 2\beta\langle S_1 S_2 I_3\rangle(t) - \gamma\langle S_1 S_2 I_3\rangle(t)
\end{aligned}
$$

$$\langle I_1 S_2 \dot{S_3} S_3 \rangle(t) = -\beta\langle I_1 S_2 S_3 I_4\rangle(t) - 2\beta\langle I_1 S_2 S_3\rangle(t) - \gamma\langle I_1 S_2 S_3\rangle(t)$$
$$\langle S_2 I_3 \dot{S_4} S_4 \rangle(t) = -\beta\langle I_1 S_2 I_3 S_4\rangle(t) + \beta\langle I_1 S_2 S_3 S_4\rangle(t) - 2\beta\langle S_2 I_3 S_4\rangle(t) - \gamma\langle S_2 I_3 S_4\rangle(t)$$
$$\langle I_1 S_2 \dot{I_4} \rangle(t) = -\beta\langle I_1 S_2 I_3 I_4\rangle(t) - 4\beta\langle I_1 S_2 I_4\rangle(t) + \beta\langle S_1 S_2 I_3 I_4\rangle(t) - 2\gamma\langle I_1 S_2 I_4\rangle(t)$$
$$\langle I_1 S_2 \dot{I_3} S_4 \rangle(t) = -6\beta\langle I_1 S_2 I_3 S_4\rangle(t) - 2\gamma\langle I_1 S_2 I_3 S_4\rangle(t)$$
$$\langle I_1 S_2 \dot{S_3} I_4 \rangle(t) = -6\beta\langle I_1 S_2 S_3 I_4\rangle(t) - 2\gamma\langle I_1 S_2 S_3 I_4\rangle(t)$$
$$\langle S_1 S_2 \dot{I_3} I_4 \rangle(t) = -6\beta\langle S_1 S_2 I_3 I_4\rangle(t) - 2\gamma\langle S_1 S_2 I_3 I_4\rangle(t)$$
$$\langle I_1 S_2 \dot{I_3} I_4 \rangle(t) = -9\beta\langle I_1 S_2 I_3 I_4\rangle(t) - 3\gamma\langle I_1 S_2 I_3 I_4\rangle(t)$$
$$\langle I_1 S_2 \dot{S_3} S_4 \rangle(t) = -3\beta\langle I_1 S_2 S_3 S_4\rangle(t) - \gamma\langle I_1 S_2 S_3 S_4\rangle(t)$$
$$\langle S_1 S_2 \dot{S_3} I_4 \rangle(t) = -3\beta\langle S_1 S_2 S_3 I_4\rangle(t) - \gamma\langle S_1 S_2 S_3 I_4\rangle(t)$$
$$\langle S_1 S_2 \dot{I_3} S_4 \rangle(t) = -3\beta\langle S_1 S_2 I_3 S_4\rangle(t) - \gamma\langle S_1 S_2 I_3 S_4\rangle(t)$$

A.2. Closed system

The system of equations with moment closures as per Theorem 2.1 describing the above SIR model on the Lollipop graph is as follows:

$$\dot{\langle S_1 \rangle}(t) = -\beta\langle S_1 I_2\rangle(t) - \beta\langle S_1 I_3\rangle(t)$$
$$\dot{\langle S_2 \rangle}(t) = -\beta\langle I_1 S_2\rangle(t) - \beta\langle S_2 I_3\rangle(t) - \beta\langle S_2 I_4\rangle(t)$$
$$\dot{\langle S_3 \rangle}(t) = -\beta\langle I_1 S_3\rangle(t) - \beta\langle I_2 S_3\rangle(t)$$
$$\dot{\langle S_4 \rangle}(t) = -\beta\langle I_2 S_4\rangle(t)$$
$$\dot{\langle I_1 \rangle}(t) = \beta\langle S_1 I_2\rangle(t) + \beta\langle S_1 I_3\rangle(t) - \gamma\langle I_1\rangle(t)$$
$$\dot{\langle I_2 \rangle}(t) = \beta\langle I_1 S_2\rangle(t) + \beta\langle S_2 I_3\rangle(t) + \beta\langle S_2 I_4\rangle(t) - \gamma\langle I_2\rangle(t)$$
$$\dot{\langle I_3 \rangle}(t) = \beta\langle I_1 S_3\rangle(t) + \beta\langle I_2 S_3\rangle(t) - \gamma\langle I_3\rangle(t)$$
$$\dot{\langle I_4 \rangle}(t) = \beta\langle I_2 S_4\rangle(t) - \gamma\langle I_4\rangle(t)$$
$$\langle S_2 \dot{I_3} \rangle(t) = -\beta\langle S_2 I_3\rangle(t)\langle S_2 I_4\rangle(t)/\langle S_2\rangle(t) - \beta\langle I_1 S_2 I_3\rangle(t) + \beta\langle I_1 S_2 S_3\rangle(t) - \beta\langle S_2 I_3\rangle(t) - \gamma\langle S_2 I_3\rangle(t)$$
$$\langle I_1 \dot{S_3} \rangle(t) = -\beta\langle I_1 I_2 S_3\rangle(t) - \beta\langle I_1 S_3\rangle(t) + \beta\langle S_1 I_2 S_3\rangle(t) - \gamma\langle I_1 S_3\rangle(t)$$
$$\langle I_2 \dot{S_3} \rangle(t) = -\beta\langle I_1 I_2 S_3\rangle(t) + \beta\langle I_1 S_2 S_3\rangle(t) - \beta\langle I_2 S_3\rangle(t) + \beta\langle S_2 I_4\rangle(t)\langle S_2 S_3\rangle(t)/\langle S_2\rangle(t) - \gamma\langle I_2 S_3\rangle(t)$$
$$\langle S_2 \dot{I_4} \rangle(t) = -\beta\langle I_1 S_2\rangle(t)\langle S_2 I_4\rangle(t)/\langle S_2\rangle(t) - \beta\langle S_2 I_3\rangle(t)\langle S_2 I_4\rangle(t)/\langle S_2\rangle(t) - \beta\langle S_2 I_4\rangle(t) - \gamma\langle S_2 I_4\rangle(t)$$
$$\langle I_1 \dot{S_2} \rangle(t) = -\beta\langle I_1 S_2\rangle(t)\langle S_2 I_4\rangle(t)/\langle S_2\rangle(t) - \beta\langle I_1 S_2 I_3\rangle(t) - \beta\langle I_1 S_2\rangle(t) + \beta\langle S_1 S_2 I_3\rangle(t) - \gamma\langle I_1 S_2\rangle(t)$$
$$\langle I_2 \dot{S_4} \rangle(t) = \beta\langle I_1 S_2\rangle(t)\langle S_2 S_4\rangle(t)/\langle S_2\rangle(t) - \beta\langle I_2 S_4\rangle(t) + \beta\langle S_2 I_3\rangle(t)\langle S_2 S_4\rangle(t)/\langle S_2\rangle(t) - \gamma\langle I_2 S_4\rangle(t)$$
$$\langle S_1 \dot{I_3} \rangle(t) = -\beta\langle S_1 I_2 I_3\rangle(t) + \beta\langle S_1 I_2 S_3\rangle(t) - \beta\langle S_1 I_3\rangle(t) - \gamma\langle S_1 I_3\rangle(t)$$
$$\langle S_1 \dot{I_2} \rangle(t) = -\beta\langle S_1 I_2 I_3\rangle(t) - \beta\langle S_1 I_2\rangle(t) + \beta\langle S_1 S_2 I_3\rangle(t) + \beta\langle S_1 S_2\rangle(t)\langle S_2 I_4\rangle(t)/\langle S_2\rangle(t) - \gamma\langle S_1 I_2\rangle(t)$$
$$\langle S_1 \dot{S_2} \rangle(t) = -\beta\langle S_1 S_2\rangle(t)\langle S_2 I_4\rangle(t)/\langle S_2\rangle(t) - 2\beta\langle S_1 S_2 I_3\rangle(t)$$
$$\langle S_2 \dot{S_4} \rangle(t) = -\beta\langle I_1 S_2\rangle(t)\langle S_2 S_4\rangle(t)/\langle S_2\rangle(t) - \beta\langle S_2 I_3\rangle(t)\langle S_2 S_4\rangle(t)/\langle S_2\rangle(t)$$
$$\langle S_2 \dot{S_3} \rangle(t) = -\beta\langle S_2 I_4\rangle(t)\langle S_2 S_3\rangle(t)/\langle S_2\rangle(t) - 2\beta\langle I_1 S_2 S_3\rangle(t)$$
$$\langle I_1 S_2 \dot{S_3} S_3 \rangle(t) = -\beta\langle I_1 S_2 S_3\rangle(t)\langle S_2 I_4\rangle(t)/\langle S_2\rangle(t) - 2\beta\langle I_1 S_2 S_3\rangle(t) - \gamma\langle I_1 S_2 S_3\rangle(t)$$
$$\langle I_1 S_2 \dot{I_3} \rangle(t) = -\beta\langle I_1 S_2 I_3\rangle(t)\langle S_2 I_4\rangle(t)/\langle S_2\rangle(t) - 4\beta\langle I_1 S_2 I_3\rangle(t) - 2\gamma\langle I_1 S_2 I_3\rangle(t)$$
$$\langle S_1 S_2 \dot{I_3} \rangle(t) = -\beta\langle S_1 S_2 I_3\rangle(t)\langle S_2 I_4\rangle(t)/\langle S_2\rangle(t) - 2\beta\langle S_1 S_2 I_3\rangle(t) - \gamma\langle S_1 S_2 I_3\rangle(t)$$
$$\langle I_1 I_2 \dot{S_3} \rangle(t) = -4\beta\langle I_1 I_2 S_3\rangle(t) + \beta\langle I_1 S_2 S_3\rangle(t)\langle S_2 I_4\rangle(t)/\langle S_2\rangle(t) - 2\gamma\langle I_1 I_2 S_3\rangle(t)$$
$$\langle S_1 I_2 \dot{S_3} \rangle(t) = -2\beta\langle S_1 I_2 S_3\rangle(t) + \beta\langle S_1 S_2 S_3\rangle(t)\langle S_2 I_4\rangle(t)/\langle S_2\rangle(t) - \gamma\langle S_1 I_2 S_3\rangle(t)$$
$$\langle S_1 I_2 \dot{I_3} \rangle(t) = -4\beta\langle S_1 I_2 I_3\rangle(t) + \beta\langle S_1 S_2 I_3\rangle(t)\langle S_2 I_4\rangle(t)/\langle S_2\rangle(t) - 2\gamma\langle S_1 I_2 I_3\rangle(t)$$
$$\langle S_1 S_2 \dot{S_3} S_3 \rangle(t) = -\beta\langle S_1 S_2 S_3\rangle(t)\langle S_2 I_4\rangle(t)/\langle S_2\rangle(t)$$

Appendix B. System for an SIR model on a path on three vertices

The following (closed) system describes the dynamics of an SIR model on a path P_3 on three vertices. The rate of infection is given by a matrix β in which $\beta_{i,j}$ gives the rate of infection from vertex i to vertex j and values γ_i give the rates of recovery for each vertex $i \in \{0,1,2\}$.

$$
\begin{aligned}
\langle \dot{S_0} \rangle &= -\beta_{1,0} * \langle S_0 I_1 \rangle \\
\langle \dot{S_1} \rangle &= -\beta_{0,1} * \langle I_0 S_1 \rangle - \beta_{2,1} * \langle S_1 I_2 \rangle \\
\langle \dot{S_2} \rangle &= -\beta_{1,2} * \langle I_1 S_2 \rangle \\
\langle \dot{I_0} \rangle &= \beta_{1,0} * \langle S_0 I_1 \rangle - \gamma_0 * \langle I_0 \rangle \\
\langle \dot{I_1} \rangle &= \beta_{0,1} * \langle I_0 S_1 \rangle + \beta_{2,1} * \langle S_1 I_2 \rangle - \gamma_1 * \langle I_1 \rangle \\
\langle \dot{I_2} \rangle &= \beta_{1,2} * \langle I_1 S_2 \rangle - \gamma_2 * \langle I_2 \rangle \\
\langle I_0 \dot{S_1} \rangle &= -\beta_{2,1} * \langle I_0 S_1 \rangle * \langle S_1 I_2 \rangle / \langle S_1 \rangle - \beta_{0,1} * \langle I_0 S_1 \rangle - \gamma_0 * \langle I_0 S_1 \rangle \\
\langle I_1 \dot{S_2} \rangle &= \beta_{0,1} * \langle I_0 S_1 \rangle * \langle S_1 S_2 \rangle / \langle S_1 \rangle - \beta_{1,2} * \langle I_1 S_2 \rangle - \gamma_1 * \langle I_1 S_2 \rangle \\
\langle S_0 \dot{I_1} \rangle &= -\beta_{1,0} * \langle S_0 I_1 \rangle + \beta_{2,1} * \langle S_0 S_1 \rangle * \langle S_1 I_2 \rangle / \langle S_1 \rangle - \gamma_1 * \langle S_0 I_1 \rangle \\
\langle S_1 \dot{I_2} \rangle &= -\beta_{0,1} * \langle I_0 S_1 \rangle * \langle S_1 I_2 \rangle / \langle S_1 \rangle - \beta_{2,1} * \langle S_1 I_2 \rangle - \gamma_{2,1} * \langle S_1 I_2 \rangle \\
\langle S_1 \dot{S_2} \rangle &= -\beta_{0,1} * \langle I_0 S_1 \rangle * \langle S_1 S_2 \rangle / \langle S_1 \rangle \\
\langle S_0 \dot{S_1} \rangle &= -\beta_{2,1} * \langle S_0 S_1 \rangle * \langle S_1 I_2 \rangle / \langle S_1 \rangle
\end{aligned}
$$

Appendix C. Proof of path system size expression

Proposition C.1. *[2] The size of the full system of equations describing an SIR model on a path graph on n vertices is* $(3n^2 - n + 2)/2$.

That is to say, the size of the full system of equations for an SIR model on a path is *quadratic* in the number of vertices in the path.

Proof. Consider an SIR model on a path graph on n vertices. Consider first the equations for single-state terms for such a system. We require an equation for each of n vertices being in states S and I, hence there are $2n$-many equations for singles.

Now, from equations for a vertex i being in state S, we require, from the master equation, two equations for each adjacent pair of vertices (i,j): $\langle S_i I_j \rangle$ and $\langle I_i S_j \rangle$, as contact with an infected vertex causes a susceptible vertex to leave this state. The remaining SI-combinations for each edge occur in the I_i equations, where the vertex i entered the infected state through being previously susceptible and coming into contact with an infected vertex. Given there are $n-1$ pairs of adjacent vertices in a path, and we require two equations for each such pair, in total there are $2(n-1)$ equations needed for two-state terms.

In the case of two-state terms of the form $\langle S_i I_j \rangle$, the only subsystem state that could lead to this state is of the form $\langle S_i S_j I_k \rangle$ for a vertex k adjacent to j (only if such a k exists i.e., j is non-terminal). States of the form $\langle S_i I_j \rangle$ could be exited by (1) the recovery of j, (2) the infection of i by j, or (3) by external infection of i. The cases of (1) and (2) do not lead to new terms as no vertices other than i and j are involved, but (3) leads to terms of the form $\langle I_h S_i I_j \rangle$ where h is a different vertex adjacent to i (if such a vertex exists). For tuples of the form $\langle I_i S_j \rangle$, the entry subsystem state is $\langle I_h S_i S_j \rangle$ for a vertex h adjacent to i. Other terms are of forms already considered in the case of states of the form $\langle S_i I_j \rangle$. Hence, all terms on three states in this system have states in the orders SSI, ISS and ISI on sub-paths of length three. There are clearly $(n-2)$-many sub-paths of length three, hence there are $3(n-2)$ equations for tuples of length three.

For tuples of length l, where $2 < l \leq n$, the number of equations is given by $3(n-(l-1))$ as, by analogous arguments to the case of $n=3$, the equations for tuples of length $l-1$ include three state combinations for tuples of length l. In particular, these are terms of the form $\langle S_i S_{i+1} \dots I_{i+(l-1)} \rangle$, $\langle I_i S_{i+1} \dots S_{i+(l-1)} \rangle$ and $\langle I_i S_{i+1} \dots I_{i+(l-1)} \rangle$, and the number of sub-paths of length l on a path is given by $(n-(l-1))$.

Hence, the total number of equations for a path on n vertices is given by

$$
\begin{aligned}
2n + 2(n-1) + 3\sum_{i=3}^{n}(n-(i-1)) &= 4n - 2 + 3\left(\sum_{i=3}^{n} n - \sum_{i=3}^{n} i + \sum_{i=3}^{n} 1\right) \\
&= 4n - 2 + 3((n-2) + (n^2 - 2n) - (n(n+1)/2 - 3)) \\
&= \frac{1}{2}(3n^2 - n + 2)
\end{aligned}
$$

which is precisely the result reported in [2]. ■

References

[1] K.J. Sharkey, Deterministic epidemic models on contact networks: correlations and unbiological terms, Theor. Popul. Biol. 79 (4) (2011) 115–129, https://doi.org/10.1016/j.tpb.2011.01.004.

[2] I.Z. Kiss, C.G. Morris, F. Sélley, P.L. Simon, R.R. Wilkinson, Exact deterministic representation of Markovian SIR epidemics on networks with and without loops, J. Math. Biol. 70 (3) (2015) 437–464, https://doi.org/10.1007/s00285-014-0772-0.

[3] R. Ross, An application of the theory of probabilities to the study of a priori pathometry-part I, Proc. R. Soc. Lond. Ser. A, Contain. Pap. Math. Phys. Character 92 (638) (1916) 204–230.

[4] W. Yang, D. Zhang, L. Peng, C. Zhuge, L. Hong, Rational evaluation of various epidemic models based on the Covid-19 data of China, Epidemics 37 (2021) 100501, https://doi.org/10.1016/j.epidem.2021.100501.

[5] Y. Liu, H. Sanhedrai, G. Dong, L.M. Shekhtman, F. Wang, S.V. Buldyrev, S. Havlin, Efficient network immunization under limited knowledge, Nat. Sci. Rev. 8 (1) (2020).

[6] W.O. Kermack, A.G. McKendrick, A contribution to the mathematical theory of epidemics, Proc. R. Soc. Lond. Ser. A, Contain. Pap. Math. Phys. Character 115 (772) (1927) 700–721.

[7] M. Dottori, G. Fabricius, SIR model on a dynamical network and the endemic state of an infectious disease, Phys. A, Stat. Mech. Appl. 434 (2015) 25–35, https://doi.org/10.1016/j.physa.2015.04.007.

[8] J. Enright, R.R. Kao, Epidemics on dynamic networks, Epidemics 24 (2018) 88–97, https://doi.org/10.1016/j.epidem.2018.04.003.

[9] D. Calvetti, A.P. Hoover, J. Rose, E. Somersalo, Metapopulation network models for understanding, predicting, and managing the coronavirus disease COVID-19, Front. Phys. 8 (2020), https://doi.org/10.3389/fphy.2020.00261.

[10] R.R. Wilkinson, K.J. Sharkey, Message passing and moment closure for susceptible-infected-recovered epidemics on finite networks, Phys. Rev. E 89 (2014) 022808, https://doi.org/10.1103/PhysRevE.89.022808.

[11] K.J. Sharkey, I.Z. Kiss, R.R. Wilkinson, P.L. Simon, Exact equations for sir epidemics on tree graphs, Bull. Math. Biol. 77 (4) (2015) 614–645, https://doi.org/10.1007/s11538-013-9923-5.

[12] K.J. Sharkey, R.R. Wilkinson, Complete hierarchies of sir models on arbitrary networks with exact and approximate moment closure, Math. Biosci. 264 (2015) 74–85, https://doi.org/10.1016/j.mbs.2015.03.008.

[13] P.L. Simon, I.Z. Kiss, On bounding exact models of epidemic spread on networks, Discrete Contin. Dyn. Syst., Ser. B 23 (5) (2018) 2005–2020.

[14] E. Otte, R. Rouirseau, Social network analysis: a powerful strategy, also for the information sciences, J. Inf. Sci. 28 (6) (2002) 441–453.

[15] D.P. Kroese, T.J. Brereton, T. Taimre, Z.I. Botev, Why the Monte Carlo method is so important today, Wiley Interdiscip. Rev.: Comput. Stat. 6 (2014).

[16] C. Kuehn, Moment Closure — a Brief Review, Control of Self-Organizing Nonlinear Systems, 2016, pp. 253–271.

[17] T.H. Cormen, C.E. Leiserson, R.L. Rivest, C. Stein, Introduction to Algorithms, 4th edition, MIT Press, 2022.

[18] A.J. Stothers, On the complexity of matrix multiplication, Ph.D. thesis, University of Edinburgh, Old College, South Bridge, Edinburgh, EH8 9YL, 2010.

[19] M. Dashtbali, M. Mirzaie, A compartmental model that predicts the effect of social distancing and vaccination on controlling COVID-19, Sci. Rep. 11 (1) (2021) 8191.

[20] A.N. Kolmogorov, Foundations of the Theory of Probability, 2nd edition, Chelsea Publishing Company, 1956.

[21] A.C. Hindmarsh, ODEPACK a systematized collection of ode solvers, IMACS Trans. Sci. Comput. 1 (1983) 55–64.

[22] L. Petzold, Automatic selection of methods for solving stiff and nonstiff systems of ordinary differential equations, SIAM J. Sci. Stat. Comput. 4 (1) (1983) 136–148.

[23] P. Erdős, A. Rényi, On random graphs I, Publ. Math. 6 (1959) 290–297.

[24] A. Gómez, G. Oliveira, New approaches to epidemic modeling on networks, Sci. Rep. 13 (1) (2023) 468.

[25] M. Newman, Networks, Oxford University Press, 2018.